JACS Au
AN OPEN ACCESS JOURNAL OF THE AMERICAN CHEMICAL SOCIETY

pubs.acs.org/jacsau
Article

Structural Studies of a Complex of a CAG/CTG Repeat Sequence-Specific Binding Molecule and A−A-Mismatch-Containing DNA

Katsuhiko Abe, Yuki Hirose, Tomotaka Kumagai, Kaori Hashiya, Kumi Hidaka, Tomoko Emura, Toshikazu Bando, Kazuki Takeda,* and Hiroshi Sugiyama*

Cite This: JACS Au 2024, 4, 1801−1810
Read Online

ACCESS | Metrics & More | Article Recommendations | Supporting Information

ABSTRACT: Triplet repeat diseases are caused by the abnormal elongation of repeated sequences comprising three bases. In particular, the elongation of CAG/CTG repeat sequences is thought to result in conditions such as Huntington's disease and myotonic dystrophy type 1. Although the causes of these diseases are known, fundamental treatments have not been established, and specific drugs are expected to be developed. Pyrrole imidazole polyamide (PIP) is a class of molecules that binds to the minor groove of the DNA duplex in a sequence-specific manner; because of this property, it shows promise in drug discovery applications. Earlier, it was reported that PIP designed to bind CAG/CTG repeat sequences suppresses the genes that cause triplet repeat diseases. In this study, we performed an X-ray crystal structure analysis of a complex of double-stranded DNA containing A−A mismatched base pairs and a cyclic-PIP that binds specifically to CAG/CTG sequences. Furthermore, the validity and characteristics of this structure were analyzed using *in silico* molecular modeling, *ab initio* energy calculations, gel electrophoresis, and surface plasmon resonance. With our direct observation using atomic force microscopy and DNA origami, we revealed that the PIP caused structural changes in the DNA strands carrying the expanded CAG/CTG repeat. Overall, our study provides new insight into PIP from a structural perspective.

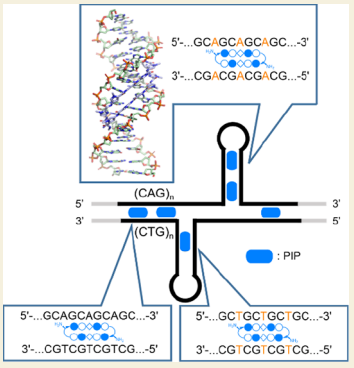

KEYWORDS: *X-ray crystal structure analysis, pyrrole imidazole polyamide, triplet repeat diseases, DNA minor groove binder, DNA origami*

INTRODUCTION

Although repeated DNA sequences are normally ubiquitous in the human genome, abnormally elongated repeat sequences can cause various diseases.[1,2] In particular, the abnormal expansion of CAG/CTG repeat sequences causes conditions such as Huntington's disease, myotonic dystrophy type 1, and spinocerebellar ataxia.[3,4] Research on compounds that bind to CAG/CTG repeat sequences for the purpose of treating these neurological diseases is progressing worldwide. Pyrrole imidazole polyamide (PIP), which is a DNA minor groove binder, was initially designed by Dickerson and colleagues based on natural DNA-binding molecules such as netropsin and distamicin.[5,6] Subsequently, Dervan and coworkers expanded the application of this compound for sequence-specific DNA recognition.[7,8] PIP consists of *N*-methylpyrrole (Py) and *N*-methylimidazole (Im) residues bound through amide bonds and recognizes duplex DNA in a sequence-specific manner. The Im−Py pair recognizes the G−C base pair, whereas the Py−Py pair recognizes both A−T and T−A base pairs. Moreover, *β*-alanine increases the flexibility of PIP and is sometimes used in place of Py; Py−*β* and *β*−*β* pairs recognize A−T or T−A pairs.[9] Using this sequence specificity, many studies have been conducted using various PIPs as drug candidates,[10,11] to visualize telomere,[12,13] and as epigenetic regulators.[14−16] A cyclic-PIP (cPIP) that strongly binds to a sequence containing CAG/CTG repeats (5′-WGCWGCW-3′, W: A or T) has been developed.[17] Furthermore, biological experiments using this cPIP revealed that it specifically binds to the hairpin structure that contains the mismatched base pairs formed thereby suppressing the genes that cause the expanded-repeat-associated diseases.[18] Although this cPIP displays a remarkable binding affinity to DNA duplexes containing canonical A−T Watson−Crick base pairs, it also exhibits a high affinity to those containing A−A or T−T mismatched base pairs, i.e., 5′-AGCAGCA-3′/3′-AGCAGCA-5′ or 5′-TGCTGCT-3′/3′-TGCTGCT-5′.[17] It has been suggested that such A−A and T−T mismatches exist in hairpin structures, which can be formed by CAG/CTG repeat sequences and are believed to be involved in the elongation of repeated sequences.[2,19] To understand the mechanism via which PIPs that target CAG/CTG sequences selectively control the expression of abnormal genes for future clinical applications, it is crucial to investigate the binding manner of

Received: December 26, 2023
Revised: March 4, 2024
Accepted: March 6, 2024
Published: May 15, 2024

PIP to double-stranded DNA (dsDNA) and its properties in detail. However, although crystallographic analyses of a complex of PIP and DNA containing only canonical base pairs have been conducted,[20,21] the crystal structure of a complex of PIP and DNA containing noncanonical base pairs, such as the A−A mismatch, has not been previously reported. Additionally, there are only few examples of crystal structure analyses of DNA strands containing A−A mismatched base pairs alone elucidated.[22−24]

In this study, we performed an X-ray crystal structure analysis of a complex of cPIP that binds to the CAG/CTG repeat sequence and DNA containing A−A mismatched base pairs. To corroborate the validity of this structure, we performed gel electrophoresis and surface plasmon resonance (SPR) tests to measure the dissociation equilibrium constants (K_d) and additionally employed *in silico* molecular modeling and *ab initio* energy calculations to verify the structural characteristics of the A−A mismatch base pairs. Moreover, we conducted an AFM study assuming that the introduction of cPIP into the nucleus leads to changes in the structure of dsDNA after it binds to the DNA strands. To verify this, we used DNA strands that mimicked an abnormally expanded CAG/CTG repeat sequence and DNA origami technology and captured the dynamic structural changes of the DNA strands in the presence of cPIP. Through these experiments, we revealed the interaction and dynamics of the cPIP at the atomic and molecular levels using both static and dynamic observation methods. Overall, our research offers novel insights into the interaction between PIP and aberrantly elongated DNA, which may have implications for the future use of PIP and related compounds in therapeutic settings.

METHODS

DNA Preparation and Crystallization

The cPIP was synthesized as previously described.[25] For forming the cPIP−DNA duplex complex, the solution containing 1.0 mM DNA duplex and 1.2 mM cPIP was annealed from 85 to 20 °C for 1 h. After 9 days, crystals were obtained in the solution of 0.50 mM cPIP−DNA duplex complex, 60 mM sodium chloride, 40 mM potassium chloride, 20 mM sodium cacodylate trihydrate pH 7.0, 20% v/v (±)-2-methyl-2,4-pentanediol, and 6.0 mM spermine tetrahydrochloride. Sitting drop method was used against a reservoir of 120 mM sodium chloride, 80 mM potassium chloride, 40 mM sodium cacodylate trihydrate pH 7.0, 40% v/v (±)-2-methyl-2,4-pentanediol, and 12 mM spermine tetrahydrochloride.

Data Collection and Crystal Structure Analysis

X-ray diffraction experiments were performed at beamline BL41XU of Spring-8 (Harima, Japan). A diffraction data set with a high redundancy was measured using X-rays with a wavelength of 0.9100 Å. In addition, the data for Br-MAD phasing were collected from the same crystal using X-rays with wavelengths of 0.9192 Å (peak), 0.9198 Å (edge-1), 0.9192 Å (edge-2), and 0.9226 Å (remote) (Table S1). Diffraction images were integrated with the XDS program.[26] The phase was determined by the MAD method (peak, edge-1, edge-2, and remote data were used) using the SOLVE/RESOLVE programs.[27,28] Four Br sites were found in the phase determination (Figure S2A). The electron density map after density modification was sufficient for model building with the Coot program (Figure S2B). The model was improved with the Coot program[29] and refined with the Phenix[30] using Translation-Libration-Screw (TLS) parameters against the high redundant data. The NCS restraints were applied between the two dsDNA−cPIP complexes through the refinement calculations other than the last few steps (Figure S2C).

In Silico Molecular Modeling

Molecular modeling studies were performed with the BIOVIA Discovery Studio (Dassault Systèmes, Vèlizy-Villacoublay, France) using a CHARMm force field. Adenines in the A−A mismatch sites were manually converted to imino adenines, T−T mismatch pairs, or A−T pairs. The complex was solvated in cubic water with 145 mM sodium chloride and premimized to maintain the interaction distance of hydrogen bonds between the polyamide part and DNA base pairs. Harmonic restraints were applied at two base pairs at both ends of DNA, and the whole structures were minimized in energy with a convergence threshold of 0.001 kcal/mol·Å in the conjugate gradient algorithm.

Ab Initio Energy Calculations

The energy levels reported here were calculated by Gaussian 16 using the Density Functional Theory (DFT) methods at B3LYP (Becke, three-parameter, Lee−Yang−Parr) and the 6-31+G* basis set. All of the calculations were carried out in the gas phase.

Polyacrylamide Gel Electrophoresis

The respective DNA strand sequences and combinations are listed in Table S2. 1−50 equiv of cPIP was added to 0.1 μM double-stranded DNA. Annealing was performed from 95 to 4 °C for 1 h in 100 mM sodium chloride and 50 mM HEPES pH 7.6 buffer. After annealing, the solutions were loaded onto an acrylamide gel (acrylamide/Bis mixed solution (29:1), Nacalai Tesque) and subjected to gel electrophoresis in 1× Tris-borate EDTA buffer at 4 °C. After electrophoresis, these gels were stained with SYBR gold nucleic acid gel stain (10,000× concentrate in DMSO) for 10 min, and gel images were observed using FAS-Digi PRO (Nippon Genetics, Tokyo, Japan). Band density was quantified using gel function of ImageJ. Based on the density of the obtained bands, the respective dissociation equilibrium constants were determined according to the following formula.[31,32] Electrophoresis was performed three times for each sequence. Three lanes were selected from each gel image to calculate the K_d value (Figure S6).

SPR Tests

SPR tests were performed on a Biacore T200 instrument (GE Healthcare) following the manufacturer's instructions. Biotinylated DNA oligomers were purchased from Japan Bio Services and immobilized on the streptavidin-functionalized SA sensor chip (GE Healthcare) to obtain the desired immobilized level (approximately 430 RU rise). SPR assays were carried out using HBS-EP buffer (10 mM HEPES pH 7.4, 150 mM sodium chloride, 3 mM EDTA, and 0.005% surfactant P20) with 0.1% DMSO at 25 °C. A series of sample solutions with various concentrations were prepared in HBS-EP buffer with 0.1% DMSO. The contact time, dissociation time, and flow rate were set for 180 s, 600 s, and 100 μL/min, respectively. The sensorgrams were fitted by using a 1:1 binding model. All sensorgrams and all values are shown in Figures S8 and 4F.

AFM Observation

All staple DNAs for the DNA origami frames were purchased from Eurofins Genomics (Tokyo, Japan). Single-stranded M13mp18 DNA was purchased from New England Biolabs (Ipswitch, MA). DNA origami frame was prepared by annealing the solution of M13mp18 DNA (final concentration of 0.01 μM), staple DNA strands (4 equiv, 0.04 μM), 20 mM Tris-HCl pH 7.6, 1 mM EDTA, and 10 mM magnesium chloride from 85 to 15 °C at a rate of −1.0 °C/min.[33] Also, CAG/CTG strands were mixed and annealed at 85 to 15 °C for 1 h to obtain 1 μM CAG/CTG bridge strands that could be cross-linked to the center of the origami. After annealing, excess staples were removed using a Sephacryl S-300 gel filtration column. 5 equiv of CAG/CTG bridge strands was added to the obtained DNA origami solution and incubated at room temperature for 1 h. Then, excess bridge strands were removed with a Sephacryl S-400 gel filtration column. Immediately before AFM observation, 50 equiv of cPIP was added. Also, as a comparative experiment, observations were made on DNA origami to which 1 nM chromomycin A3 was added. Origami with bridge strand and cPIP were imaged on a high-speed AFM

https://doi.org/10.1021/jacsau.3c00830
JACS Au 2024, 4, 1801−1810

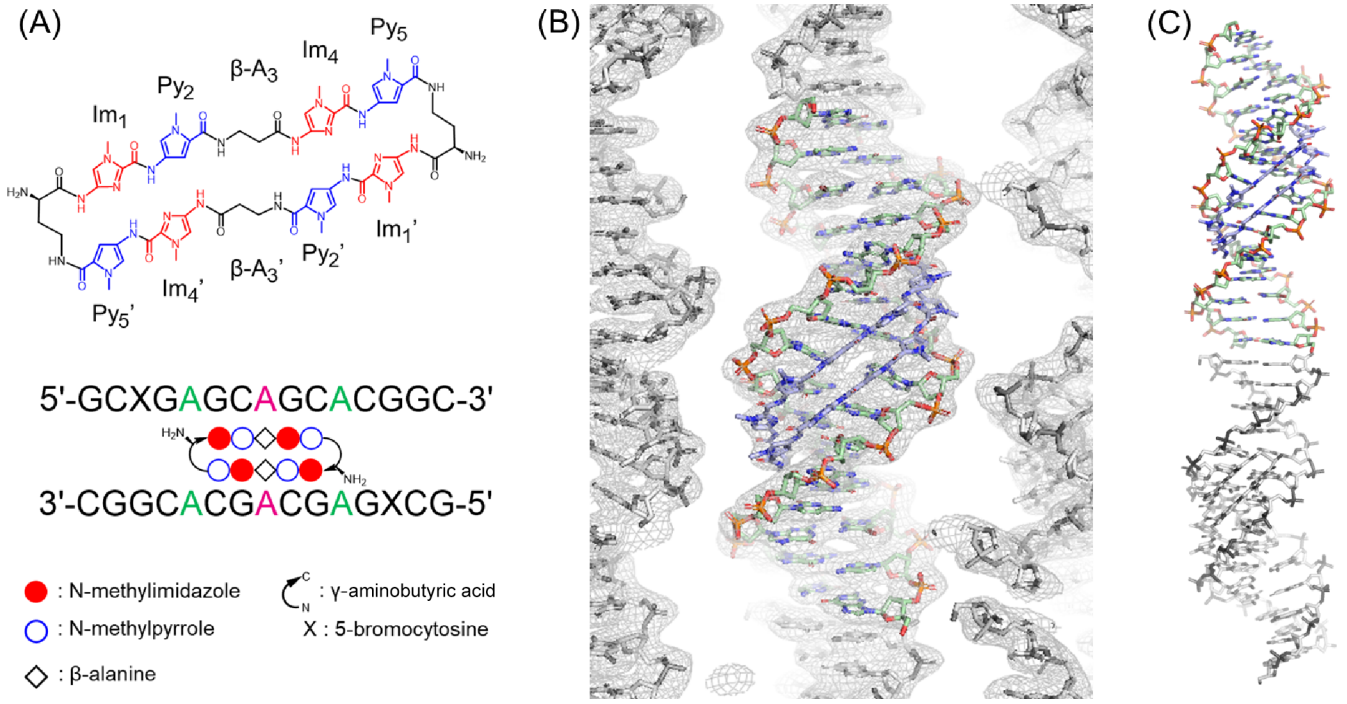

Figure 1. Chemical structure of cPIP and results of the structural analysis. (A) Chemical structure and ball-and-stick annotation of a cPIP targeting the 5′-WGGWCCW-3′ sequence. This cPIP can bind to DNA with A−A mismatches. (B) The crystal structure of the cPIP−DNA complex. A sigma-Aweighted 2*Fo*−*Fc* map is shown at a contour level of 1 σ. (C) Two complexes within an asymmetric unit. One complex is colored, whereas the other is presented in gray.

(Nano-Live Vision; RIBM, Tsukuba, Japan). The incubated sample (2 μL) was absorbed on a freshly cleaved mica plate for 5 min at room temperature and then washed with buffer solution for the observation of a single conformational change directly. Scanning was performed in a 130 μL buffer solution containing 20 mM Tris (pH7.6) and 10 mM magnesium chloride using a small cantilever (Ultra-Short Cantilevers USC-F0.8-K0.1-T12, NanoWorld, Neuchâtel, Switzerland). When origami was adhered to mica, 0.1% 3-aminopropyltriethoxysilane (APTES) was added after regular incubation of origami, and further incubation was performed for 5 min. AFM images were obtained at a rate of 0.2 frames per second.

RESULTS AND DISCUSSION

Characteristics of cPIP and DNA Strands with a CAG Sequence Containing A−A Mismatched Base Pairs

In this study, we prepared a DNA strand with a palindromic structure containing the CAG repeat sequence and synthesized a cPIP that binds to this sequence based on previous research (Figure 1A).[17] This cPIP recognizes the 5′-WGCWGCW-3′ sequence. Moreover, the palindromic DNA strands formed a self-dimer, resulting in a 15-mer DNA duplex containing three A−A mismatched base pairs (two terminal A_5−A_{11} pairs and a central A_8−A_8 pair). In addition to G−C-specific Im−Py pairs, the β−β pair and γ-turns of PIP recognize this A−A mismatch, resulting in the specificity of the cPIP for this sequence.

Structure of the cPIP−DNA Complex with a CAG Sequence Containing A−A Mismatched Base Pair

The cPIP−DNA complex was crystallized and subjected to an X-ray structure analysis. The space group of the crystal was $P2_12_12_1$. We determined the structure using multiwavelength anomalous diffraction method based on the anomalous scattering effect of bromine atoms, which were incorporated into the DNA strand as bromocytosine (Figure 1B and Table 1, PDB ID: 8WU5). The crystal contained two cPIP−DNA

Table 1. Data Collection and Structure Refinement Statics

PBD ID: 8WU5	
	refined data
Diffraction Data	
space group	$P2_12_12_1$
cell dimensions	
a, *b*, *c*, Å	27.18, 44.05, 194.3
α, β, γ, °	90, 90, 90
wavelength, Å	0.9100
resolution, Å	50−2.80 (2.97−2.80)
R_{merge}[a], %	11.3 (970.4)
$\langle I/\sigma(I)\rangle$[a]	20.18 (0.56)
$CC_{1/2}$[a], %	100.0 (83.2)
completeness[a],%	100.0 (99.9)
no. of unique reflections[b]	6280 (973)
redundancy	74.5 (76.8)
Refinement	
resolution, Å	50−2.80
R_{work}/R_{free}, %[c]	28.42/29.66
no. of atoms	
DNA	1228
polyamide B	192
B factors, Å^2	
DNA	167.27
polyamide B	151.10
r.m.s.d.[d]from ideal	
bond length, Å	0.012
bond angles, °	1.251

[a]Values for the highest-resolution shell are in parentheses. [b]Bijvoet pairs were kept separate. [c]R_{free} was calculated using 5% of the reflections that were not included in the refinement as a test set. [d]Root-mean-square deviation.

https://doi.org/10.1021/jacsau.3c00830
JACS Au 2024, 4, 1801−1810

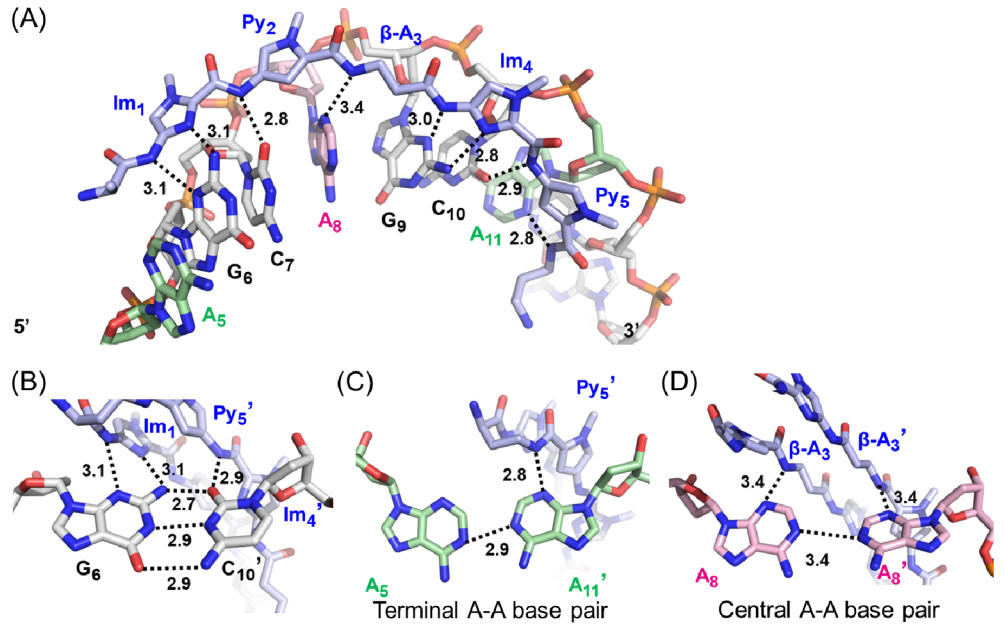

Figure 2. Interaction between DNA bases and cPIP. (A) Imidazoles and amides interact with bases of dsDNA through 16 hydrogen bonds. (B) Interactions by hydrogen bonding between Im−Py and G−C pairs. (C) Interaction by hydrogen bonding between the amide of Im−Py and the terminal A−A mismatch base pair. (D) Interaction by hydrogen bonding between the *β*-alanine moieties of cPIP and the central A−A mismatch pair.

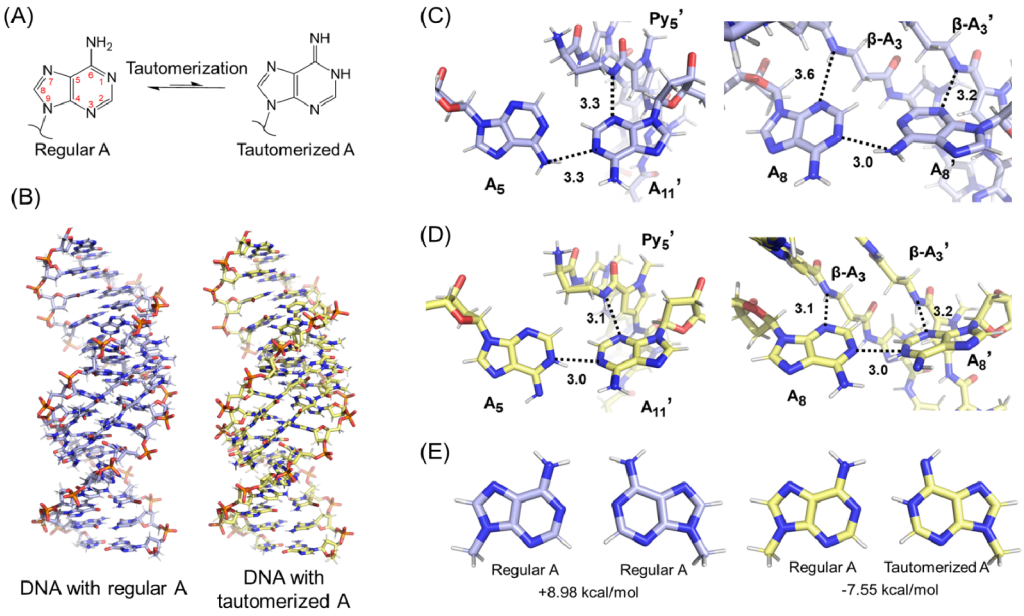

Figure 3. Consideration of the noncanonical base pair structure in A−A mismatches. (A) Schematic representation of the tautomerization of adenine. In the tautomerized adenine, the N1 atom is hydrogenated. (B) Structures obtained after *in silico* molecular modeling (BIOVIA Discovery Studio using a CHARMm force field) with or without the tautomerization of adenine. An enlarged view of the central A−A base pair of each structure is shown in parts C and D. The two structures did not change significantly after structural analysis. (C) Result of *in silico* modeling without assuming adenine tautomerization. Unlike the crystal structure, the interatomic distance between the N1 atom and the amine at the 6th position was smaller. (D) Result of the *in silico* modeling assuming adenine tautomerization. Similar to the results of the structural analysis, both adenines were stabilized by directing the N1 atoms to each other. (E) Results of the *ab initio* energy calculation of the A−A base pair and A−tautomerized A base pair. The energy levels were calculated using the DFT method at B3LYP/6-31+G* levels.

complexes in the asymmetric unit. After the final refinement, the R_{work} and R_{free} values converged to 28.42% and 29.66%, respectively, at a resolution of 2.80 Å. The two DNA structures exhibited an almost identical conformation with an RMSD of 0.62 Å. Moreover, a comparison with the regular B-form DNA strand revealed that the minor groove was greatly expanded due to the binding of the cPIP (Figure S4). This expansion can be considered a common feature as it is also observed in earlier cPIP−DNA complexes.[20,21]

Interactions Between cPIP and DNA Bases

The interaction between cPIP and DNA bases was next examined based on the obtained crystal structure. Each of the

https://doi.org/10.1021/jacsau.3c00830
JACS Au 2024, 4, 1801−1810

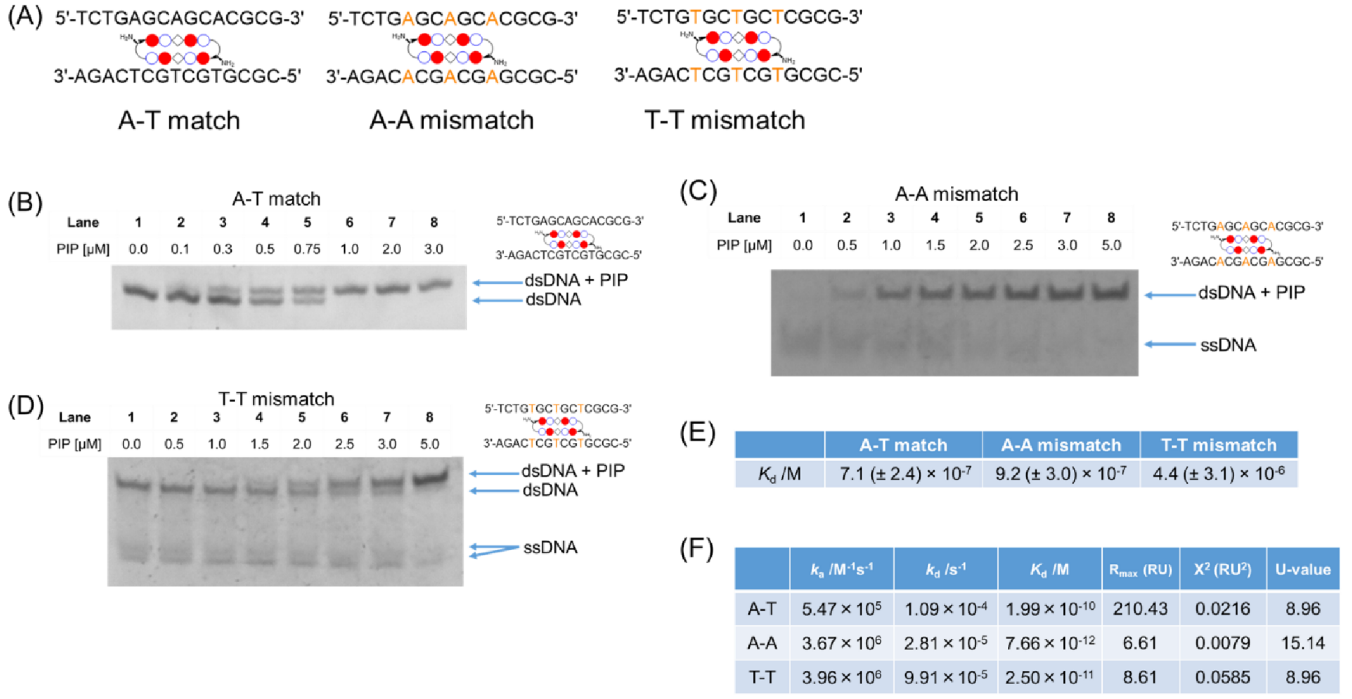

(E)

	A-T match	A-A mismatch	T-T mismatch
K_d /M	7.1 (± 2.4) × 10^{-7}	9.2 (± 3.0) × 10^{-7}	4.4 (± 3.1) × 10^{-6}

(F)

	k_a /$M^{-1}s^{-1}$	k_d /s^{-1}	K_d /M	R_{max} (RU)	X^2 (RU^2)	U-value
A-T	5.47 × 10^5	1.09 × 10^{-4}	1.99 × 10^{-10}	210.43	0.0216	8.96
A-A	3.67 × 10^6	2.81 × 10^{-5}	7.66 × 10^{-12}	6.61	0.0079	15.14
T-T	3.96 × 10^6	9.91 × 10^{-5}	2.50 × 10^{-11}	8.61	0.0585	8.96

Figure 4. Determination of dissociation equilibrium constants (K_d) by gel electrophoresis. (A) Sequences of the DNA strands used and assumed binding positions of cPIP. (B) Gel electrophoresis of DNA strands containing A−T matched base pairs and cPIP. The DNA concentration was 0.1 μM. K_d values were determined by using the results from lanes 3 to 5. Gel electrophoresis of DNA strands containing (C) A−A mismatch or (D) T−T mismatch base pairs and PIP. The concentration of DNA strand was 0.1 μM in terms of double strands. K_d values were determined using the results from lanes 4 to 6. (E) K_d values calculated based on the density of each band. (F) The summary of analysis data by SPR tests for a cPIP with dsDNA contains A−T match base pairs, A−A mismatch base pairs, or T−T mismatch base pairs. R_{max} is the maximal binding amount when the analyte (cPIP) occupies all of the immobilized ligand (DNA). The theoretical R_{max} can be calculated using the following formula: R_{max} = molecular weight of the analyte (Da) × immobilized amount of the ligand (RU) × number of binding sites/molecular weight of the ligand (Da).

four DNA strands in the asymmetric unit had the same sequence, and the cPIP also had a 2-fold axis of symmetry; therefore, the structures of four almost-equivalent half-PIP−single-stranded DNAs were contained in these two cPIP−dsDNA complexes (Figure 2A). The cPIP recognized the dsDNA through a total of 16 hydrogen bonds. Both the G−C base pairs, and the terminal A−A mismatches were recognized by the cPIP with hydrogen bonds of 2.8−3.1 Å, and it was inferred from the bond distance that only the central adenine was recognized by a longer hydrogen bond (3.4 Å). Regarding the G−C base pair, two hydrogen bonds were formed between the Im unit and guanine, and one hydrogen bond was formed between the Py unit and cytosine; moreover, guanine and cytosine were forming regular base pairs (Figure 2B). These findings are consistent with the recognition mode observed in other PIP−DNA complexes.[20,21,34] Subsequently, the terminal A−A base pairs were recognized by the nitrogen on the amide bond at the γ-turn of cPIP. In addition, the distance (2.9 Å) between the two nitrogen atoms at position 1 (N1 atoms) of the A−A base pair implied the presence of an interaction via hydrogen bonding, even though these atoms normally do not form a hydrogen bond (Figure 2C). To create a stable structure in such a state, hydrogen bonds must be formed with the appropriate interatomic distances and angles. It is known that, when adenine tautomerizes, the N1 atom is hydrogenated (Figure 3A).[35] It is plausible that the tautomerization of one adenine in the A−A base pair contributes to the formation of a stable structure without distortion by hydrogen bonds between the bases and between each base and cPIP (Figure 3). Finally, with regard to the central A−A mismatch, it seems that a hydrogen bond was formed between the N3 atom on adenine and the nitrogen atom on β-alanine, although the distance was slightly large (Figure 2D). In addition, it is assumed that hydrogen bonds are formed between adenines based on the principle described above, and it can be said that these three hydrogen bonds contribute to the stabilization of the structure. The crystal structure obtained in this instance showed that a stable dsDNA was formed with the adenines facing each other, mediated by cPIP.

In Silico Molecular Modeling and *Ab Initio* Energy Calculations Regarding A−A Mismatch Bases

With respect to the interaction between adenines, we hypothesized the presence of a tautomerized adenine (Figure 3A). To verify this, we conducted *in silico* molecular modeling and *ab initio* energy calculation. For the terminal mismatch, the adenine that did not interact with cPIP was manually tautomerized in the model, whereas for the central mismatch, where both adenines interacted with cPIP, the modeling was run with one tautomerized adenine. We also prepared a control model without tautomerized adenine and compared the two models. Both structures maintained a double-stranded structure, and the cPIPs also existed in positions similar to those of the original structure (Figure 3B). When only regular adenine was used, the modeling structure showed that the N1 atom and the amine at position 6 were sufficiently close to form a hydrogen bond, which was different from that observed in the crystal structure (Figure 3C). Conversely, in the case of DNA with tautomerized adenine, the N1 atoms faced each other, similar to the results of the crystal structure analysis (Figure 3D). Furthermore, because the model that was

https://doi.org/10.1021/jacsau.3c00830
JACS Au 2024, 4, 1801−1810

prepared using tautomerized adenine exhibited a structure that was closer to the obtained crystal structure than that obtained using only regular adenine, it seems more natural to assume the presence of base pairs consisting of a regular and a tautomerized A base.

To examine the stability of the regular and tautomerized adenine base pairs, *ab initio* energy calculations were performed. The atomic position of the A−A base pair obtained from the crystal structure was fixed in the calculations. When the base pair of regular adenine was assumed exclusively, it was found that a structure with the N1 atoms facing each other was energetically disadvantageous (+8.98 kcal/mol) (Figure 3E). Subsequently, the energy calculation revealed that a base pair of the regular and tautomerized adenine was more energetically stable than the free single bases due to the interactions between base pairs (−7.55 kcal/mol). Thus, to obtain a structure in which the N1 atoms of adenine face each other, as in the crystal structure, it is reasonable from an energetic point of view to consider the tautomerization of one adenine.

Structural analyses of the A−A mismatched base pairs that have been reported revealed that, in dsDNA that does not interact with other molecules, a hydrogen bond formed between the N1 atom and the amine at the sixth position (Figure S5A).[24] Conversely, there is an example in which a DNA strand incorporating tetrahydrofuran interacted with a protein, resulting in a structure in which the N1 atoms of adenine faced each other (Figure S5B).[23] In our crystal structure, because of the intervention of cPIP, the adenine exhibited a structure in which a hydrogen bond was formed with the nitrogen on cPIP, and this interaction fixed the position of the adenines. The results of this crystallographic analysis, *in silico* modeling, *ab initio* calculations, and previous research[23,24] suggest that the cPIP may contribute to adenine tautomerization and facilitate noncanonical base pairing. To our best knowledge, there is no study reporting the pairing of multiple irregular bases between adenines in regular dsDNA that has been demonstrated by X-ray crystallographic analysis until now.

Binding Affinity of cPIP to DNA Strands

The cPIP used in this research exhibits a high binding affinity for not only DNA strands containing A−A mismatched base pairs but also DNA strands containing A−T matches and T−T mismatches.[17,18] In previous studies, the melting temperature (T_m) was mainly used for interpretation, but it reveals only the thermodynamic stability of DNA.[17] The dissociation equilibrium constant (K_d) of the cPIP toward DNA strands containing A−A mismatches and T−T mismatches was not determined yet. To get more insight on the cPIP interaction toward DNA, we performed gel electrophoresis.

For gel electrophoresis, DNA strands containing A−T match, A−A mismatch, or T−T mismatch base pairs were annealed with various concentrations of cPIP and loaded onto a polyacrylamide gel (Figure 4A). The analysis of A−T matched strands revealed an upward band shift in the presence of the cPIP (Figure 4B). This corresponded to the increase in molecular weight caused by the binding of the cPIP. Regarding the A−A mismatched dsDNA, the results of electrophoresis revealed that the addition of the cPIP caused the previously single-stranded DNA to become double-stranded (Figure 4C). This indicates that the A−A mismatched region was stabilized, and that duplex formation was promoted through the intervention of the cPIP, which is consistent with our crystal structure. Our electrophoresis run also revealed that the T−T mismatched strands formed a double-stranded structure before the addition of the cPIP compared with the A−A base pair (Figure 4D). We assume that this can be attributed to the purine bases facing each other in the A−A base pair, while the T−T base pair had small pyrimidine bases facing each other. Furthermore, the lower steric hindrance due to the smaller pyrimidine bases can also be presumed to have promoted duplex formation. Furthermore, in all cases, as the concentration of the cPIP increased, the intensity of the lower band visibly reduced, while an increase in the intensity of the upper band was observed (Figure S6). This indicates that the proportion of dsDNA increased with the addition of the cPIP. The determination of the K_d values from the results reported above revealed that the binding was stronger in the order of A−T match > A−A mismatch > T−T mismatch (Figure 4E). Moreover, in the case of A−A mismatched base pairs, the results of the electrophoresis showed that the DNA, which was in the single-stranded DNA state in the absence of the cPIP, formed a double strand after the addition of the cPIP. This implies that this cPIP promotes the formation of duplexes by stabilizing the typical unstable mismatched base pairs.

Our crystal structure and molecular modeling can add further insights into our assumption from the gel electrophoresis. In the obtained crystal structure, the central A−A mismatch pair was replaced with an A−T or T−T base pair, and *in silico* molecular modeling was conducted. In the A−T base pair, a total of four hydrogen bonds were formed between cPIP and each base and between the bases. Also, it was found that the bases and the cPIP were spatially arranged in a positional relationship that did not cause steric hindrance (Figure S7A). In the case of T−T base pair, the bases and the cPIP are also in a positional relationship that does not cause high steric hindrance (Figure S7B). However, because the distance between the bases is too large to form a hydrogen bond, it is thought that two hydrogen bonds in total were formed only between the cPIP and the bases. From the results of crystal structure analysis, a total of three hydrogen bonds are formed in the central A−A mismatch base pair area (Figure 2D). From these results, it can be inferred that the number of hydrogen bonds could be related to the strength of the binding of cPIP to dsDNA. In this way, by combining the crystal structure obtained in this study with modeling, we were able to obtain new insights into the binding constant.

From our gel electrophoresis, we were able to confirm the change in DNA strand stability due to the cPIP in an equilibrium state. To kinetically investigate cPIP binding and dissociation over time, we performed measurements using SPR (Figures S8 and 4F). From our SPR test, the R_{max} for the DNA strands with A−T match base pairs alone was higher than the expected value (∼40 RU), and the other values were generally within the analysis range. The high R_{max} value may be due to the linearity of the binding region. In addition, the K_d value calculated for the A−T match sequence of the same cPIP in the previous study was about 10 times larger,[17] but the accuracy of the fitting appears to be higher in the present data. Regarding the dsDNA containing A−A mismatch or T−T mismatch, although a low R_{max} was detected, other values were appropriate, similar to the case of the A−T match. Note that the sensorgram in the dissociated area is considered to be close to horizontal and susceptible to baseline drift, so we took care while making comparisons. However, unlike the results of gel electrophoresis, a comparison of K_d values showed that the

https://doi.org/10.1021/jacsau.3c00830
JACS Au 2024, 4, 1801−1810

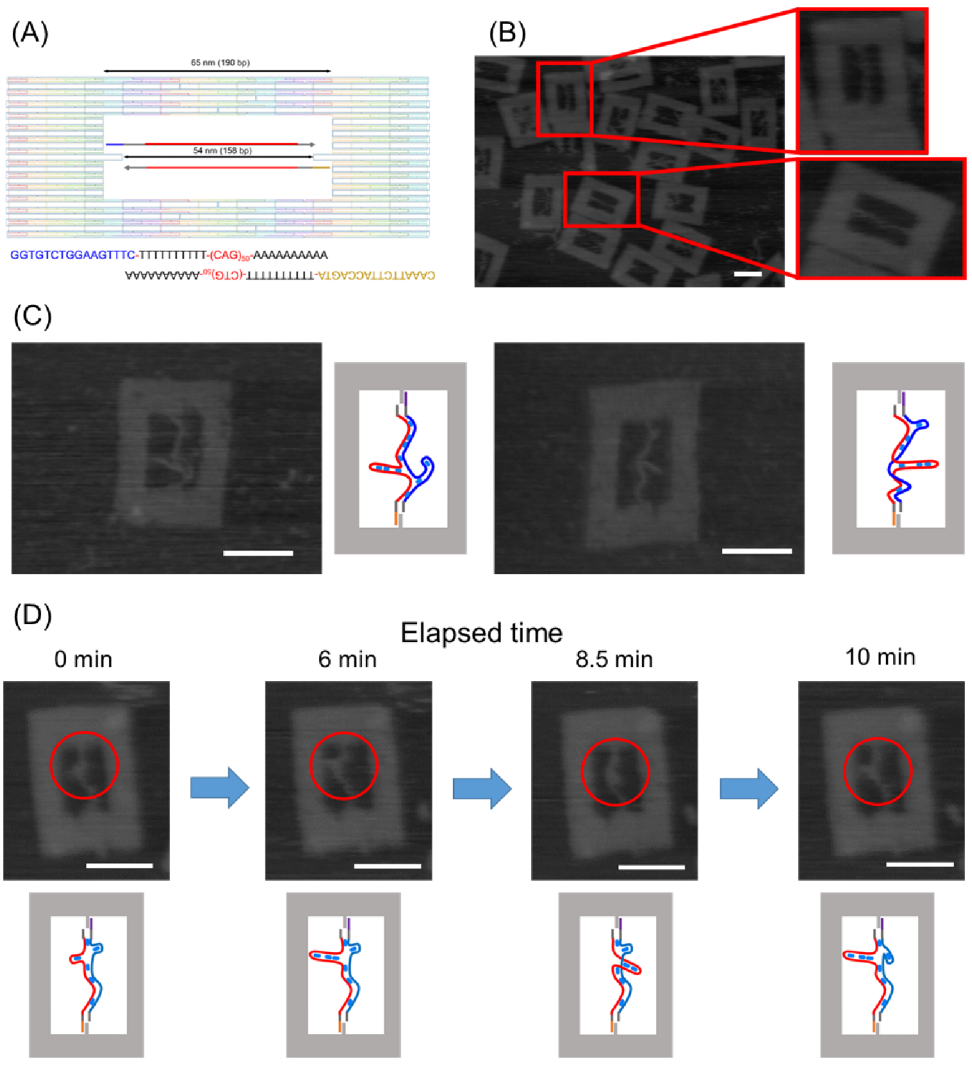

Figure 5. AFM observation of structural changes in DNA strands induced by cPIP binding. (A) Schematic diagram of the DNA origami used for this observation and the DNA strand arrangement that mimicked the CAG/CTG repeat sequence. (B) Origami and cross-linked DNA before adding cPIP. DNA strands have a nearly linear structure. (C) State of the DNA strand after adding cPIP. The branched structure is induced by cPIP. Schematic diagrams of the assumed DNA strand are shown to the right of the AFM images. For a clearer observation of the structure, 3-aminopropyltriethoxysilane (APTES) processing was performed. (D) The branching structure dynamically changed and moved. (B–D) Scale bars: 50 μm.

binding of the cPIP to A–A mismatched dsDNA had the highest binding ability and that of the cPIP to A–T matched dsDNA had the lowest binding ability. The results of electrophoresis showed that the binding was stronger in the order A–T match > A–A mismatch > T–T mismatch (Figure 4E). The difference between the results of electrophoresis and SPR can be assumed that while electrophoresis observes the equilibrium-reached system, SPR observes the process leading to equilibrium over time. In addition, while two DNA strands were used in electrophoresis, the cPIP was bound to intrastrand hairpin structure in SPR. Due to these factors, it is possible that the evaluation of binding ability differs between the two experiments. Furthermore, the SPR results suggested that this cPIP may exhibit a different binding sequence preference under conditions where kinetic effects prevail than when equilibrium is achieved.

Observation of the Structural Changes Caused by the Interaction Between CAG/CTG Repeat Sequences and cPIP Using DNA Origami and hsAFM

Previous research has demonstrated the therapeutic potential of the cPIP we studied in treating CAG/CTG repeat-related triplet diseases.[18] It is crucial to investigate and elucidate its interactions and dynamics toward the repeat sequences in order to consider it as a viable clinical candidate. We were able to obtain important insights into its affinity toward dsDNA through our crystallography and binding kinetics experiments. In order to gain a deeper understanding of the molecular-level dynamic interactions of this cPIP with the DNA sequence, we employed atomic force microscopy (AFM). Leveraging our laboratory's previous experience with DNA origami, we utilized high-speed AFM (hsAFM) to study the dynamic interactions of biomolecules at a molecular level.[33,36,37]

Thereby, employing DNA origami and AFM, we observed the structural changes caused by the addition of the cPIP to DNA strands that mimicked the CAG repeat sequence (Figure

https://doi.org/10.1021/jacsau.3c00830
JACS Au 2024, 4, 1801–1810

5A).[33] The DNA strands contained 50 repeats of CAG/CTG repeated sequences. In the absence of the cPIP, DNA strands with an unbranched structure were observed (Figure 5B and Supporting Video 1), whereas in the presence of the cPIP, DNA strands with a branched structure were observed (Figure S9). Among them, some images with more clearly visible branching structures are shown, accompanied by illustrations of plausible structures of the cPIP-induced intrastrand duplex that could have resulted in the shapes seen within the cavity of the DNA origami frame (Figure 5C). At this time, two or more branched structures were observed, which seemed to correspond to the observation that each CAG/CTG strand stably forms a hairpin structure. In addition, we observed dynamic structural changes several minutes after the addition of the cPIP (Figure 5D and Supporting Video 2). Here, the observation was performed for about 10 min, with the time at which observation started being set to 0 min. At the initial time point, the branching of the DNA strands was negligible and not distinct. However, over time, the branching became clearer (after 6 min), and we were able to observe dynamic movement from side to side and up and down (after 8.5 min). This branched structure was retained even after 10 min, indicating that it was not a temporary structure that appeared by chance. In addition, as a comparative experiment, in the presence of chromomycin A3, which binds to CG-rich sequences, DNA strands without a branched structure were observed, similar to the case of the absence of the cPIP (Figure S10 and Supporting Video 3). These results suggest that this cPIP dynamically changes linear dsDNA to a branched structure. Also, SPR results suggested that this cPIP may prefer binding to mismatched regions rather than to matched regions. The presence of the cPIP allows mismatched base pairs to exist thermodynamically more stably even in long DNA chains, which is why the branched structure was observed in hsAFM. Another reason for the formation of branched structures due to the cPIP is that the binding of the cPIP to match base pairs may change the structure of the DNA strands and accumulate distortion. Additionally, since the DNA strands are fixed in origami, there is a possibility that the DNA strands will be further distorted, and it is thought that the DNA strands will be more likely to form a branched structure to resolve this distortion. Thus, the hsAFM results may also suggest that the hairpin structure was generated due to complex factors and that the ability of this cPIP for stabilization to mismatch base pair was exerted, which cannot be determined by the K_d value alone. Furthermore, distortion also occurs in DNA strands within the nucleus due to nucleosome formation, transcription, and replication. Therefore, based on the structure observed in this experiment, it will be helpful to consider the structural changes to DNA strands caused by PIP in the nucleus. Although the existence of this branching structure was hypothesized in a previous study,[18] this was the first direct observation of such a structure. We believe by observing the dynamic interaction between PIP and DNA, we can better understand how it behaves inside cells and pave the way for future studies in this area. Furthermore, the presence of these branched structures, as shown here, makes it plausible to target them in future studies and may provide an impetus for developing new strategies.

CONCLUSION

In this study, a cPIP that specifically binds to CAG/CTG repeat sequences bound to dsDNA containing A−A mismatch base pairs, and the binding mode was confirmed by X-ray crystallography. To the best of our knowledge, no crystal structural data have been obtained for DNA containing multiple A−A mismatched base pairs. Therefore, the recognition of not only the usual G−C base pair but also definite hydrogen bonding to the A−A mismatch was confirmed. It has also been suggested that hydrogen bonds, which do not normally appear, occur between adenines; the crystal structure analysis and modeling performed here revealed that this may be attributed to the tautomerization of one adenine. In addition, an experiment aimed at determining the dissociation equilibrium constants suggested significantly strong binding between cPIP and sequences containing A−A and T−T mismatched base pairs. Furthermore, through experiments using DNA origami and AFM, it was directly observed for the first time that cPIP significantly changes the structure of DNA strands containing CAG/CTG repeat sequences. By considering these results comprehensively, we were able to provide new insights into the behavior of PIP within the nucleus. We believe that our results contribute to the field of the design, *in silico* modeling, and simulation of various small and medium-sized molecules, including PIP, for triplet diseases.

ASSOCIATED CONTENT

Supporting Information

The Supporting Information is available free of charge at https://pubs.acs.org/doi/10.1021/jacsau.3c00830.

Experimental procedures, data of X-ray crystal structure and density map, and results of SPR sensorgrams, *in silico* modeling, and AFM observation; the HPLC spectrum and MALDI-TOF MS of the compound (Figure S1); the X-ray crystal structure of reverse binding orientation cPIP−DNA duplex complex (Figure S2); 2*Fo-Fc* map attached to the main structure (Figure S3); comparison of cPIP−DNA complex to regular DNA (Figure S4); comparison of hydrogen bonding between A−A mismatch base pair (Figure S5); graphs showing the ratio of the cPIP-bound DNA strands band to the total band in electrophoresis for each sequence (Figure S6); *in silico* molecular modeling for A−T or T−T base pair based on the crystal structure (Figure S7); the SPR sensorgrams for a cPIP with dsDNA (Figure S8); AFM observation of structural changes in DNA strands induced by cPIP binding without fixation by APTES (Fgiure S9) and treated with chromomycin A3 without fixation with APTES (Figure S10); data collection and structure refinement statics (Table S1); summary of conditions for acrylamide electrophoresis for each double strand (Table S2) (PDF)

Supporting video of AFM observation 1 (absence of cPIP) (MP4)

Supporting video of AFM observation 2 (presence of cPIP) (MP4)

Supporting video of AFM observation 3 (presence of chromomycin A3) (MP4)

AUTHOR INFORMATION

Corresponding Authors

Kazuki Takeda − *Department of Chemistry, Graduate School of Science, Kyoto University, Kyoto 606-8502, Japan;*

https://doi.org/10.1021/jacsau.3c00830
JACS Au 2024, 4, 1801−1810

orcid.org/0000-0002-4094-6816; Email: ktakeda@kuchem.kyoto-u.ac.jp

Hiroshi Sugiyama − *Institute for Integrated Cell-Material Science (WPI-iCeMS), Kyoto University, Kyoto 606-8501, Japan*; orcid.org/0000-0001-8923-5946; Email: sugiyama.hiroshi.3s@kyoto-u.ac.jp

Authors

Katsuhiko Abe − *Department of Chemistry, Graduate School of Science, Kyoto University, Kyoto 606-8502, Japan*

Yuki Hirose − *Department of Chemistry, Graduate School of Science, Kyoto University, Kyoto 606-8502, Japan*; orcid.org/0000-0002-2956-071X

Tomotaka Kumagai − *Department of Chemistry, Graduate School of Science, Kyoto University, Kyoto 606-8502, Japan*

Kaori Hashiya − *Department of Chemistry, Graduate School of Science, Kyoto University, Kyoto 606-8502, Japan*

Kumi Hidaka − *Department of Chemistry, Graduate School of Science, Kyoto University, Kyoto 606-8502, Japan*

Tomoko Emura − *Department of Chemistry, Graduate School of Science, Kyoto University, Kyoto 606-8502, Japan*

Toshikazu Bando − *Department of Chemistry, Graduate School of Science, Kyoto University, Kyoto 606-8502, Japan*

Complete contact information is available at: https://pubs.acs.org/10.1021/jacsau.3c00830

Author Contributions

CRediT: **Katsuhiko Abe** investigation.

Notes

The authors declare no competing financial interest.

■ ACKNOWLEDGMENTS

We thank Dr. Kei Okatsu and Dr. Syuya Fukai (Department of Chemistry, Graduate School of Science, Kyoto University) for helping in SPR assay. This research was supported by JSPS KAKENHI (JP21J22721, Grant-in-Aid for JSPS Fellows to K.A., 20H05936 and 21H04705 to H.S.). For *in silico* molecular modeling studies, computation time was provided by the Super Computer System, Institute for Chemical Research, Kyoto University. We also thank the beamline staff at BL41XU of SPring-8 for their help with the diffraction experiments (proposal no. 2021B2533 and 2022A2533 to K.T.).

■ REFERENCES

(1) Mirkin, S. M. Expandable DNA Repeats and Human Disease. *Nature* **2007**, *447* (7147), 932−940.

(2) Usdin, K.; Grabczyk, E. Review DNA Repeat Expansions and Human Disease. *Cell. Mol. Life Sci.* **2000**, *57* (6), 914−931.

(3) Guan, L.; Disney, M. D. Covalent Small-Molecule−RNA Complex Formation Enables Cellular Profiling of Small-Molecule−RNA Interactions. *Angew. Chem.* **2013**, *125* (38), 10194−10197.

(4) Nakatani, K.; Hagihara, S.; Goto, Y.; Kobori, A.; Hagihara, M.; Hayashi, G.; Kyo, M.; Nomura, M.; Mishima, M.; Kojima, C. Small-Molecule Ligand Induces Nucleotide Flipping in (CAG)n Trinucleotide Repeats. *Nat. Chem. Biol.* **2005**, *1* (1), 39−43.

(5) Kopka, M. L.; Yoon, C.; Goodsell, D.; Pjura, P.; Dickerson, R. E. Binding of an antitumor drug to DNA: Netropsin and C-G-C-G-A-A-T-T-^{Br}C-G-C-G. *J. Mol. Biol.* **1985**, *183*, 553−563.

(6) Kopka, M. L.; Yoon, C.; Goodsell, D.; Pjura, P.; Dickerson, R. E. The Molecular Origin of DNA-Drug Specificity in Netropsin and Distamycin. *Proc. Natl. Acad. Sci. U. S. A.* **1985**, *82*, 1376−1380.

(7) Dervan, P. B.; Edelson, B. S. Recognition of the DNA Minor Groove by Pyrrole-Imidazole Polyamides. *Curr. Opin. Struct. Biol.* **2003**, *13* (3), 284−299.

(8) Dervan, P. B.; Bürli, R. W. Sequence-Specific DNA Recognition by Polyamides. *Curr. Opin. Chem. Biol.* **1999**, *3*, 688−693.

(9) Turner, J. M.; Swalley, S. E.; Baird, E. E.; Dervan, P. B. Aliphatic/Aromatic Amino Acid Pairings for Polyamide Recognition in the Minor Groove of DNA. *J. Am. Chem.* **1998**, *120* (2), 6219−6226.

(10) Morita, K.; Suzuki, K.; Maeda, S.; Matsuo, A.; Mitsuda, Y.; Tokushige, C.; Kashiwazaki, G.; Taniguchi, J.; Maeda, R.; Noura, M.; et al.et al. Genetic Regulation of the RUNX Transcription Factor Family Has Antitumor Effects. *J. Clin. Invest.* **2017**, *127* (7), 2815−2828.

(11) Erwin, G. S.; Grieshop, M. P.; Ali, A.; Qi, J.; Lawlor, M.; Kumar, D.; Ahmad, I.; Mcnally, A.; Teider, N.; Worringer, K.; et al.et al. Synthetic Transcription Elongation Factors License Transcription across Repressive Chromatin. *Science* **2017**, *358*, 1617−1622.

(12) Tsubono, Y.; Kawamoto, Y.; Hidaka, T.; Pandian, G. N.; Hashiya, K.; Bando, T.; Sugiyama, H. A Near-Infrared Fluorogenic Pyrrole−Imidazole Polyamide Probe for Live-Cell Imaging of Telomeres. *J. Am. Chem. Soc.* **2020**, *142* (41), 17356−17363.

(13) Kawamoto, Y.; Sasaki, A.; Chandran, A.; Hashiya, K.; Ide, S.; Bando, T.; Maeshima, K.; Sugiyama, H. Targeting 24 bp within Telomere Repeat Sequences with Tandem Tetramer Pyrrole−Imidazole Polyamide Probes. *J. Am. Chem. Soc.* **2016**, *138* (42), 14100−14107.

(14) Taniguchi, J.; Feng, Y.; Pandian, G. N.; Hashiya, F.; Hidaka, T.; Hashiya, K.; Park, S.; Bando, T.; Ito, S.; Sugiyama, H. Biomimetic Artificial Epigenetic Code for Targeted Acetylation of Histones. *J. Am. Chem. Soc.* **2018**, *140* (23), 7108−7115.

(15) Ohtsuki, A.; Kimura, M. T.; Minoshima, M.; Suzuki, T.; Ikeda, M.; Bando, T.; Nagase, H.; Shinohara, K.-I.; Sugiyama, H. Synthesis and properties of PI polyamide−SAHA conjugate. *Tetrahedron Lett.* **2009**, *50* (52), 7288−7292.

(16) Nickols, N. G.; Dervan, P. B. Suppression of Androgen Receptor-Mediated Gene Expression by a Sequence-Specific DNA-Binding Polyamide. *Proc. Natl. Acad. Sci. U. S. A.* **2007**, *104* (25), 10418−10423.

(17) Hirose, Y.; Ohno, T.; Asamitsu, S.; Hashiya, K.; Bando, T.; Sugiyama, H. Strong and Specific Recognition of CAG/CTG Repeat DNA (5′-DWGCWGCW-3′) by a Cyclic Pyrrole-Imidazole Polyamide. *ChemBiochem* **2022**, *23* (2), No. e202100533.

(18) Ikenoshita, S.; Matsuo, K.; Yabuki, Y.; Kawakubo, K.; Asamitsu, S.; Hori, K.; Usuki, S.; Hirose, Y.; Bando, T.; Araki, K.; et al.etal. A Cyclic Pyrrole-Imidazole Polyamide Reduces Pathogenic RNA in CAG/CTG Triplet Repeat Neurological Disease Models. *J. Clin. Invest.* **2023**, *133* (22), No. e164792.

(19) Gacy, A. M.; Goellner, G.; Juranić, N.; Macura, S.; McMurray, C. T. Trinucleotide Repeats That Expand in Human Disease Form Hairpin Structures in Vitro. *Cell* **1995**, *81*, 533−540.

(20) Chenoweth, D. M.; Dervan, P. B. Allosteric Modulation of DNA by Small Molecules. *Proc. Natl. Acad. Sci. U. S. A.* **2009**, *106* (32), 13175−13179.

(21) Abe, K.; Hirose, Y.; Eki, H.; Takeda, K.; Bando, T.; Endo, M.; Sugiyama, H. X-ray Crystal Structure of a Cyclic-PIP−DNA Complex in the Reverse-Binding Orientation. *J. Am. Chem. Soc.* **2020**, *142* (23), 10544−10549.

(22) Zeglis, B. M.; Pierre, V. C.; Kaiser, J. T.; Barton, J. K. A Bulky Rhodium Complex Bound to an Adenosine-Adenosine DNA Mismatch: General Architecture of the Metalloinsertion Binding Mode. *Biochemistry* **2009**, *48* (20), 4247−4253.

(23) Fairlamb, M. S.; Whitaker, A. M.; Freudenthal, B. D. Apurinic/Apyrimidinic (AP) Endonuclease 1 Processing of AP Sites with 5′Mismatches. *Acta Crystallogr., Sect. D: Struct. Biol.* **2018**, *74*, 760−768.

(24) MacDonald, D.; Demarre, G.; Bouvier, M.; Mazel, D.; Gopaul, D. N. Structural Basis for Broad DNA-Specificity in Integron Recombination. *Nature* **2006**, *440* (7088), 1157−1162.

(25) Asamitsu, S.; Kawamoto, Y.; Hashiya, F.; Hashiya, K.; Yamamoto, M.; Kizaki, S.; Bando, T.; Sugiyama, H. Sequence-specific DNA alkylation and transcriptional inhibition by long-chain hairpin pyrrole−imidazole polyamide−chlorambucil conjugates targeting CAG/CTG trinucleotide repeats. *Bioorg. Med. Chem.* **2014**, *22* (17), 4646−4657.
(26) Kabsch, W. XDS. *Acta Crystallogr., Sect. D: Struct. Biol.* **2010**, *66* (2), 125−132.
(27) Terwilliger, T. C.; Berendzen, J. Biological Crystallography Auto-mated MAD and MIR Structure Solution. *Acta Crystallogr., Sect. D: Struct. Biol.* **1999**, *55*, 849−861.
(28) Terwilliger, T. C. Terwilliger Maximum-Likelihood Density Modification Biological Crystallography Maximum-Likelihood Density Modification. *Acta Crystallogr., Sect. D: Struct. Biol.* **2000**, *D56*, 965−972.
(29) Emsley, P.; Lohkamp, B.; Scott, W. G.; Cowtan, K. Features and Development of Coot. Acta. *Crystallogr. D Biol. Crystallogr.* **2010**, *66* (4), 486−501.
(30) Afonine, P. V.; Grosse-Kunstleve, R. W.; Echols, N.; Headd, J. J.; Mori-Arty, N. W.; Mustyakimov, M.; Terwilliger, T. C.; Urzhumtsev, A.; Zwart, P. H.; Adams, P. D. Towards Automated Crystallographic Structure Refinement with Phenix.Refine. *Acta Crystallogr. D Biol. Crystallogr.* **2012**, *68* (4), 352−367.
(31) Heddi, B.; Cheong, V. V.; Martadinata, H.; Phan, A. T. Insights into G-quadruplex specific recognition by the DEAH-box helicase RHAU: Solution structure of a peptide−quadruplex complex. *Proc. Natl. Acad. Sci. U. S. A.* **2015**, *112* (31), 9608−9613.
(32) Yu, Z.; Guo, C.; Wei, Y.; Hashiya, K.; Bando, T.; Sugiyama, H. Pip-HoGu: An Artificial Assembly with Cooperative DNA Recognition Capable of Mimicking Transcription Factor Pairs. *J. Am. Chem. Soc.* **2018**, *140* (7), 2426−2429.
(33) Raghavan, G.; Hidaka, K.; Sugiyama, H.; Endo, M. Direct Observation and Analysis of the Dynamics of the Photoresponsive Transcription Factor GAL4. *Angew. Chem.* **2019**, *131* (23), 7708−7712.
(34) Chenoweth, D. M.; Dervan, P. B. Structural Basis for Cyclic Py-Im Polyamide Allosteric Inhibition of Nuclear Receptor Binding. *J. Am. Chem. Soc.* **2010**, *132* (41), 14521−14529.
(35) Guerra, C. F.; Bickelhaupt, F. M.; Saha, S.; Wang, F. Adenine Tautomers: Relative Stabilities, Ionization Energies, and Mismatch with Cytosine. *J. Phys. Chem. A* **2006**, *110* (11), 4012−4020.
(36) Räz, M. H.; Hidaka, K.; Sturla, S. J.; Sugiyama, H.; Endo, M. Torsional Constraints of DNA Sub-strates Impact Cas9 Cleavage. *J. Am. Chem. Soc.* **2016**, *138* (42), 13842−13845.
(37) Endo, M.; Xing, X.; Zhou, X.; Emura, T.; Hidaka, K.; Tuesuwan, B.; Sugiyama, H. Single-Molecule Manipulation of the Duplex Formation and Dissociation at the G-Quadruplex/i-Motif Site in the DNA Nanostructure. *ACS Nano* **2015**, *9* (10), 9922−9929.

https://doi.org/10.1021/jacsau.3c00830
JACS Au 2024, 4, 1801−1810